Multiple conformations of full-length p53 detected with single-molecule fluorescence resonance energy transfer

Fang Huang[*,†], Sridharan Rajagopalan[*,†], Giovanni Settanni[*], Richard J. Marsh[§], Daven A. Armoogum[§], Nick Nicolaou[§], Angus J. Bain[§], Eitan Lener[¶], Elisha Haas[¶], Liming Ying[‖] and Alan R. Fersht[*,§§]

[*]MRC Centre for Protein Engineering, Hills Road, Cambridge, CB2 0QH, UK.

[§]Department of Physics and Astronomy, University College London, Gower Street, London, UK WC1E 6BT

[¶]The Goodman Faculty of life sciences, Bar-Ilan University, Ramat Gan Israel, 52900.

[‖] Molecular Medicine, National Heart and Lung Institute, and Chemical Biology Centre, Imperial College London, London, SW7 2AZ, UK.

[§§]Corresponding author

Email: arf25@cam.ac.uk

Fax: 44-1223-402-140

[†]These authors contributed equally.

Abstract

The tumour suppressor p53 is a member of the emerging class of proteins that have both folded and intrinsically disordered domains, which are a challenge to structural biology. Its N-terminal domain (NTD) is linked to a folded core domain, which has a disordered link to the folded tetramerization domain, which is followed by a disordered C-terminal domain. The quaternary structure of human p53 has been solved by a combination of NMR spectroscopy, electron microscopy and small-angle x-ray scattering (SAXS), and the NTD ensemble structure by NMR and SAXS. The murine p53 is reported to have a different quaternary structure, with the N- and C-termini interacting. Here, we employed single-molecule fluorescence resonance energy transfer (SM-FRET) to investigate the conformational dynamics of the NTD of p53 in isolation and in the context of tetrameric full-length p53. Our results showed that the isolated NTD was extended in solution with a strong preference for residues 66-86 forming a polyproline II (PPII) conformation. The NTD associated weakly with the DNA binding domain of p53, but not the C-termini. We detected multiple conformations in full-length p53 that were likely to result from the interactions of NTD with the DNA binding domain of each monomeric p53. Overall, the SM-FRET results, in addition to corroborating the ensemble findings, uniquely resolved the intrinsic dynamics of p53, which are often averaged and lost in conventional ensemble techniques. Our study presented here, exemplifies the usefulness of SM-FRET in exploring the dynamic landscape of multimeric proteins that contain regions of unstructured domains.

Keywords: p53, natively disordered, domain-domain interaction, single-molecule, FRET

\body

The tumor suppressor p53 is a tetrameric, multi-domain transcription factor that plays key roles in maintaining the integrity of the human genome and in DNA repair machinery (1, 2). p53 is a partly intrinsically disordered protein (IDP), containing two folded domains: the DNA-binding core domain (CD, residues 94-294); and the tetramerization domain (TetD, residues 323-360) (3, 4). The intrinsically disordered N-terminal transactivation domain (NTD, residues 1-94) and C-terminal negative regulatory domain (CTD, residues 360-393) (5, 6) mediate interactions with several proteins such as p300/CBP, MDM2, 14-3-3 and S100 family that in turn regulate the activity of p53. Moreover, the NTD and CTD are the target sites of numerous post-translational modificiations that modulate the activity of p53.

High-resolution structures of the CD and the TetD have been solved using x-ray crystallography and NMR spectroscopy (3, 4, 7, 8). But, the intrinsic instability, and the presence of highly disordered regions in p53 have impeded the application of conventional structural studies on full-length p53 (flp53). A combination of NMR spectroscopy and small-angle x-ray scattering (SAXS) in solution with electron microscopy on immobilised samples was recently used to solve the quaternary structures of a mutationally stabilised human flp53 and its DNA complex (9). The ensemble structure of the NTD has further been analysed in solution by residual dipolar couplings and SAXS (10). A radically different structure has been proposed from cryoelectron microscopy studies on murine p53 in which the N- and C-termini are suggested to interact (11).

We applied single-molecule fluorescence resonance energy transfer (SM-FRET) (12, 13) and time-resolved FRET (TR-FRET) (14) techniques to gain further information on the quaternary structure of p53, the disposition of its disordered

regions and domain-domain interactions. The unique advantage of SM-FRET over ensemble-averaged measurements is that it allows us to segregate the heterogeneity of a complex ensemble, which is especially important in assigning structure-function relationship to proteins that are conformationally mobile, such as the denatured state of proteins (15-18). Owing to its unique advantages, SM-FRET has been widely applied to monitor structural changes (19-22), dynamics (23) and molecular interactions of biomolecules (24). However, there are only a few studies to date on large multi-domain proteins and protein complexes using SM-FRET (25-27). This paucity is possibly due to the difficulty of selective and specific labelling, the distance limitations of FRET measurements and the inherent complexity (such as stability) of the systems. Recent advancements with larger Förster critical distance donor/acceptor pairs and the development of more sophisticated alternating excitation techniques have allowed to extend the distance limitations (28). While large dyes are used in these systems, TR-FRET allows the use of small fluorescence probes to study protein dynamics and conformational distribution (29). Based on the SM-FRET and TR-FRET experiments, we discuss our results in the context of the inherent conformational heterogeneity present in a single tetrameric p53 molecule while bringing in the consistencies observed between ensemble and single molecule measurements.

Results

Establishing the FRET system

As there are no Cys residues in the NTD of p53, we introduced Cys residues as labelling anchors for FRET studies at different positions so that distances between different residues could be measured: p53N(1C91C) (M1C W91C); p53N(10C56C)

(V10C E56C); and p53N(56C91C) (E56C W91C). The two Cys of each mutant were labelled with Alexa Fluor 488 (= AF488, FRET donor) and Alexa Fluor 647 (= AF647, FRET acceptor) randomly, i.e., the position of the donor and the acceptor may exchange. Random labelling has been adopted throughout the study for all the samples under investigation. To check the effect of random labelling, we used the B-domain of Protein A (BDPA) as a control, where we can introduce labels either selectively or randomly (21). The similarity of the histograms for the selectively and randomly labelled BDPA showed that this exchange did not affect noticeably the SM-FRET efficiency histogram.

The Förster critical distance (R_0) for AF488/AF647 is ~52 Å, which allows distances between 42 Å and 66 Å, corresponding to FRET efficiency of 0.8 and 0.2, respectively, to be accurately measured. For much larger or much smaller distances, the measurement becomes insensitive and may introduce large errors. To measure larger distances, we used another donor/acceptor pair, Alexa Fluor 546/Alexa Fluor 647 (AF546/AF647), which has a Förster critical distance of 63 Å. The Förster critical distances, we measured, are different from those reported by Invitrogen (56 Å and 74 Å for AF488/AF647 and AF546/AF647, respectively), probably due to the change in the fluorescence quantum yield and spectra upon labelling.

flp53 has 10 Cys residues, three of which are buried and involved in Zn^{2+} co-ordination (Cys-176, Cys-238 and Cys-242). Some of the other seven Cys residues are buried or partly exposed, Cys-124, Cys-135, Cys-141 and Cys-275, while the exposed residues include Cys-182, Cys-229 and Cys-277 (30). To avoid mislabelling, we mutated all the exposed and partly exposed Cys to Ala, i.e., C124A, C182A, C275A and C277A. We used two mutant forms of p53 harbouring labelling positions in the NTD and the DNA binding domain (56C229C and 56C292C). For the mutant p53

(56C292C), we mutated Cys-229 to Ala. These mutations were introduced in the tetrameric full length p53 (flp53, 1-393) and a monomeric construct lacking the oligomerization and C-terminal regulatory domain (p53NCD, 1-292), for labelling and subsequent single molecule experiments. FRET pairs AF488/AF647 and AF546/AF647 were used for all mutants. The protein and DNA binding control experiments showed that the mutant p53 and wild-type p53 had similar DNA and protein binding constants, suggesting that the dyes had little effect on the protein functionality and structure (*c.f.* Supporting Information for details).

Distance between residues in the NTD of p53 using SM-FRET

p53N(10C56C) and p53N(56C91C) with AF488 as FRET donor and AF647 as acceptor gave a single peak (apart from the Zero peak) in the SM-FRET efficiency histogram at FRET efficiency of 0.45 and 0.41, respectively (Fig. 1). The single peak pattern of the SM-FRET efficiency histogram suggested that there was only one ensemble of conformations that could be observed in the NTD of p53. No peak was observed in between 0.2 and 1 in the SM-FRET efficiency histogram of p53N(1C91C), suggesting the distance between residues 1 and 91 was too large for the AF488/AF647 pair as any peak with FRET efficiency <0.2 is not resolvable with our setup (because of the strong Zero peak). Using AF546 as a FRET donor, the histogram peak shifted from low to high FRET efficiency. The peak for p53N(10C56C) and p53N(56C91C) shifted to 0.61 and 0.53, respectively (Table 1). A peak at 0.25 for p53N(1C91C) was also observed, due to the larger Förster critical distance for the AF546/AF647 pair. The apparent average distance between dyes was calculated with the FRET efficiency at the peak using the equation $r = \left(1/E_{peak} - 1\right)^{1/6} R_0$. The apparent average distances obtained from AF546/AF647 system were greater than those obtained from the AF488/AF647 system (Table 1).

This reflects the broad distance distribution of the flexible NTD. Previous work (31) suggests that a systematic positive deviation would be observed in a loose flexible system when a steady-state FRET technique is applied and the Förster critical distance is longer than the distance to be measured, i.e. $R_0 > r$, while a negative deviation would be expected when $R_0 < r$. The systematic deviation is minimized when the FRET efficiency is close to 0.5. Since the FRET efficiency for p53N(10C56C) and p53N(56C91C) was slightly smaller than 0.5 when AF488 was used as donor and slightly greater than 0.5 when AF546 acted as donor, the actual distance should be in between the values obtained with these two donor/acceptor pairs, i.e., 54-58 Å for p53N(10C56C) and 56-62 Å for p53N(56C91C). For p53N(1C91C), the FRET efficiency was only 0.25, a negative deviation is, therefore, expected, i.e. the actual distance may be greater than 76 Å. Assuming that the NTD is an ideal chain, the radius of gyration (R_g) can be calculated from the FRET end-to-end distance with the equation $R_g = r/\sqrt{6}$, where r is the end-to-end distance. The calculated R_g value of 31.0 Å is similar to the value obtained from SAXS experiments (27 Å) (H. Tidow and ARF, personal communication). The slightly greater value from FRET may result from the linker between the dye and the protein but may also be an indication of the non-ideal chain behaviour of the NTD, caused by the high helix propensity of the proline-rich region (10).

Distance between residues in the NTD of p53 using TR-FRET

To get average distances and the distance distribution between residues in the NTD of p53, we synthesized a series of short peptides: residues 1-17 (p53N1-17), residues 14-30 (p53N14-30), residues 62-78 (p53N62-78) and residues 74-92 (p53N74-92) (*c.f.* Supporting Information for sequences). In the peptides p53N1-17, p53N62-78 and p53N74-92, naphthylalanine (Nal-Ala) at C-terminus was used as FRET donor and 5-

(((acetylamino)ethyl)amino) naphthalene-1-sulfate (EDANS) at N-terminus acted as FRET acceptor. This pair has a Förster critical distance of 22 Å. Peptide p53N14-30 has Trp at position 23, which has similar excitation and emission spectra to those of naphthylalanine. To avoid the influence of the fluorescence from Trp on FRET measurement, we used another donor-acceptor pair of EDANS/Dabsyl (4-dimethylaminoazobenzene-4'-sulfonyl), which has a Förster critical distance of 30 Å. Time-resolved fluorescence spectra of the FRET donor were acquired in the presence and absence of FRET, which were then fitted numerically to a differential equation using a skewed Gaussian as radial distribution function (*cf.* Supporting Information). The equilibrium distance distributions are shown in Fig. 2 (*cf.* Fig. S1 in Supporting Information for the fit of raw data) and all the fitted parameters were listed in Table 2. No obvious systematic deviations were found in the residuals (*cf.* Supporting information) and a more complex model (two skewed Gaussian radial distribution function) did not improve the χ^2 significantly, while the random coil model (Gaussian model) also provided larger χ^2 values. The same data were also fitted with another program (32) with and without acceptor signal to check for any fitting errors. We could not improve the determination of the parameters by global fitting with both the donor and the acceptor decay data. The fitting without using the acceptor signal gave similar results as shown in Table 2 (*cf.* Table S1 in Supporting Information). All the peptides gave broad end-to-end distance distributions, which suggested all the peptides truncated from NTD do not have a rigid conformation, supporting the notion that NTD is intrinsically disordered (5, 10). The distance distribution of the p53N1-17 peptide was narrower than the other peptides and peaked at a smaller value. The distance distributions of the p53N14-30, p53N62-78 and p53N74-92 were very similar. The similarity between the three peptides may be due to their propensity to

form helical secondary structure (10, 33). The high helix propensity for p53N74-92 was consistent with the circular dichroism spectrum, which showed clear characteristics of PPII structure, i.e. a positive peak at 227 nm (See Fig. S2 in Supporting Information). The circular dichroism spectra for the other peptides did not show any obvious evidence for secondary structure, which, however, does not exclude the possibility for the existence of residual secondary structures. Although indication for PPII structure was observed (10), the end-to-end distance of p53N62-78 and p53N74-92 was significantly shorter than expected from ideal PPII structure (similar to results from SM-FRET data of p53N(56C91C)). The existence of *cis*-proline (34, 35) and flexible residues (36) may significantly decrease the end-to-end distance observed by FRET. A compacted conformation of PPII forming peptides is also observed with other techniques (37). All the four peptides gave very small intramolecular diffusion coefficient values, which are much smaller than the reported values for very flexible peptides (38, 39) but similar to the values observed for other protein's internal chain segments (40). It is reasonable to observe a very small diffusion coefficient due to the presence of Pro residues in p53N1-17 (4 Pro), p53N62-78 (6 Pro) and p53N74-92 (8 Pro), the α-helix formation propensity of p53N14-30 and the strong sequence dependence of peptide flexibility (36, 41).

SM-FRET efficiency histogram of the monomeric subunit of p53

The NTD plus CD of p53 (p53NCD, residues 1-292) does not contain the TetD and the unstructured C-terminus and is a paradigm for studying the behaviour of monomeric p53. The SM-FRET efficiency histogram of the p53NCD gave a single broad peak (apart from the Zero peak) (Fig. 3) for both the FRET pair mutants studied. When AF488/AF647 were used, its peak centred at a FRET efficiency of 0.63

for p53NCD(56C229C) and 0.60 for p53NCD(56C292C), corresponding to apparent average distances of 48±2 and 49±2 Å, respectively. Larger apparent average distances were obtained when AF546/AF647 were used for similar reasons discussed above (Table 1). Since the deviation can be minimized and neglected when the FRET efficiency is close to 0.5, apparent average distance values corresponding to FRET efficiency close to 0.5 are, therefore, regarded to closer to the actual mean distances. We therefore took 48±2 Å and 49±2 Å as the apparent average distances between fluorophores in p53NCD(56C229C) and p53NCD(56C292C), respectively.

It is very interesting to observe smaller apparent average distances between the dyes in the p53NCD (~48-49 Å) than that in the isolated p53N(56C91C) (56-62 Å). This was a clear indication of an interaction between the NTD and CD, as the inter-dye distance in isolated NTD is expected to be smaller than that in p53NCD without this interaction. The NTD is extended and highly flexible in solution and possibly exists in a dynamic equilibrium between the free state and the bound state where NTD associates with CD. The single peak appearing in the SM-FRET efficiency histogram could arise from either i) multiple conformational ensembles that exchange faster than 1 ms^{-1} (hence not resolvable on SM time scale) or ii) two (or more) ensembles with slow exchange rate but either one has much greater distances and so is not observable in SM-FRET experiments or the ensembles have similar FRET efficiency and, therefore, give a broad peak. To distinguish the possibilities clearly, further investigation will be required, as for example using alternating excitation SM-FRET, which can detect longer distances (28).

Quaternary structure of flp53 and domain-domain interactions

To explore the quaternary structure of flp53 and potential domain-domain interactions, we prepared several mutants: flp53(56C229C); flp53(56C292C);

flp53(2C229C); and flp53(2C394C), all of which were based on the quadruple Cys→Ala mutant construct. To avoid FRET between different monomers within the same tetramer, the concentration of labelled protein and the unlabelled protein was controlled to be ~100 pM and ~1 μM, respectively, so that the chance of observing tetramers with 2 labelled subunits is statistically insignificant. SM-FRET experiments for flp53(2C229C) suggested that the N-terminus of the NTD is distant from the CD since no peak with FRET efficiency between 0.2 to 1 was observed when AF488/AF647 were used. Similarly, no peak was observed in between 0.2 and 1 in the SM-FRET efficiency histogram of flp53(2C394C), when AF488/AF647 or AF546/AF647 were used, which suggested that the distance between the two ends of the flp53 was at least greater than 80 Å. This experiment excluded the possibility of interactions between the N- and C-termini within the same monomer. We then designed another experiment to probe any possible interaction between the N- and C-termini of different monomers in the same tetramer. The concentration of the labelled protein, 100 pM, is too low to form tetramers in the single-molecule experiments since the dissociation constant of tetrameric p53 to dimers is ~100 nM (42). We designed bulk-measurements to maintain labelled p53 at tetrameric levels. In the new flp53 mutant, we introduced the tetracysteine motif (CCPGCC) to the C-terminus of p53, through which ReAsH (a fluorescent dye selectively labels CCPGCC, from Invitrogen) was labelled to the protein with close to 100% labelling efficiency (43). AF488 was then introduced to Cys-2 as FRET donor to establish a FRET system with ReAsH, which gives a Förster critical distance of 59 Å (calculated from fluorescence quantum yield and spectral overlap). A FRET efficiency of $0.04^{+0.08}_{-0.02}$ was obtained from the steady-state fluorescence intensity measurements, corresponding to an apparent average distance of 100 ± 20 Å. Since there are 4 acceptors in a tetramer

with a FRET donor, this experiment suggested that the distance between the N-terminus and any of the C-termini in the same tetramer was greater than 100 ± 20 Å and hence excluded the possibility of N- and C- termini interactions between different subunit. While Okorokov et al (11) propose that the N and C-termini of murine p53 interact within a tetramer, our FRET study clearly showed no indication of such interactions within the human protein. The FRET result is consistent with the previous SAXS model of p53 (9) but different from the cryoelectron microscopy results (11).

The SM-FRET histogram of both flp53(56C229C) and flp53(56C292C) showed multiple peaks and broad distribution (Fig. 4), implying multiple conformations for the flp53 that interconvert in > 1 ms. The multiple peaks cannot be assigned to FRET between different monomers within the same tetramer since it was experimentally excluded by controlling the concentration of the labelled and unlabelled protein (as mentioned above). The labelling sites for p53NCD and corresponding flp53 are exactly the same, but the histograms are obviously different, suggesting the organisation of the domains is different in the presence and absence of the TetD and CTD. p53NCD gave apparently only one peak between 0.2 and 1 in the SM-FRET efficiency histogram. This peak, although still present in the SM-FRET efficiency histogram for flp53, was flanked with new peaks appearing at higher and lower FRET efficiency. The comparison of the histograms of p53NCD and flp53 (Fig. 3 and Fig. 4) strongly suggested that tetramerization influenced the relative position of the NTD and the CD significantly. If the NTD interacts with the CD, it is more likely that it not only binds to the CD from the same monomer but also to the CDs from the other monomers within the same tetramer since the NTD is long and flexible enough to make contacts with CD's of other subunits (Fig. 5). TetD plays an important role in bringing the CDs close in space for a proximal interaction with NTDs. In the simplest

scenario, if the NTD binds to all the CDs in the same tetramer differentially, then four different conformations with different distances would be expected (Fig. 5), which would reflect by the appearance of multiple peaks in the SM-FRET efficiency histogram. Since the peak observed in the SM-FRET efficiency histogram for the p53NCD corresponds to the NTD-CD interacting conformer, the distance between position 56 and 229 or 292 in full-length p53 may even be shorter when the NTD interacts with the neighbouring CDs.

Extensive control experiments using fluorescence correlation spectroscopy (FCS) and time-resolved fluorescence anisotropy were carried out (*c.f.* Supporting Information for details). These experiments supported the conclusion that the multiple peaks observed in the single molecule FRET histogram were evidence for the existence of sub-populations of conformers but not a result of protein aggregates or restricted fluorophores, as observed in previous work with protein-chaperone interactions (44),

Discussion

The SM-FRET studies are consistent with the previous structural work on human flp53, have confirmed that the N- and C-termini are very far apart, have revealed structural details about the NTD and have detected weak interactions that were not visible to bulk measurements.

Expanded NTD

It has been proposed that the Proline-rich region in the NTD forms PPII structure (10). The mean end-to-end distance obtained for the synthetic peptide derived from the Proline-rich region (residues 74-92) was much shorter than the expected distance for a PPII structure with the same number of residues, probably because of the presence of *cis*-Pro or flexible residues in this region. For both residual dipolar couplings and

SAXS experiments, a population of less than 20% of *cis*-Pro would be at the limit of detection. Conversely, SM-FRET and TR-FRET yield detailed distributions of distances and subpopulations. This enables detection of minor conformers. Moreover, the r^{-6} dependence of FRET efficiency allows, when proper pairs of dyes are used, to emphasize the contribution of minor conformations. The SM-FRET experiments showed that the apparent end-to-end distance of the NTD was large, suggesting an extended NTD in isolation. The N-terminus of NTD was found to be distant from the CD, which is in agreement with the results obtained from the SAXS experiments (9). On the other hand, an obvious indication for the existence of interactions between the NTD and the CD was obtained from the observation of shorter distance between residues 56 and 229 (or 292) in the p53NCD than between residues 56 and 91 in isolated NTD. The experiments further suggested that the NTD interacted with CD with a correlation time > 1 ms. This interaction seemed not to significantly reduce the radius of gyration of the whole molecule and it means that the NTD maintains loose and flexible characteristics. It is known that NTD can act as ssDNA mimic and the isolated NTD interacts weakly with isolated CD (45).

Multiple conformations of flp53

The observation of multiple peaks in the SM-FRET efficiency histogram provided direct evidence for the existence of multiple conformations of flp53, which did not exchange on time scale shorter than 1 ms. Whereas only a single but broad peak was observed in the SM-FRET efficiency histogram for p53NCD, we obtained complex histograms for full-length p53, indicative of effects of forming the tetramer. NMR experiments suggest that the structure of the CD does not change upon tetramerization (46). TetD holds p53 as a loosely packed dimer of dimers, making the NTD of each monomer accessible to the CD of the other monomers in a tetrameric subunit resulting

in multiple conformations (Fig. 5). The FRET data reported here showed the existence of weak interactions between the NTD and the CDs within the same tetramer, which are not directly detectable in NMR experiments (46).

The FRET results were, in general, consistent with the proposed structure of full-length p53 (9). The interaction between the NTD and the CD observed in the SM-FRET experiments was not detected in the SAXS experiments, which localized only the quaternary structures of the folded domains, and measured the overall radius of gyration, which is insensitive to the disordered N-termini. Since both the SAXS and FRET experiments suggested that the NTD has a very extended conformation even in the presence of CD, the interaction between NTD and CD is probably weak. However such interactions may play a functional role in mediating interactions with other proteins or with response elements.

Acknowledgment

S.R. is supported by a fellowship from the Cambridge Commonwealth Trust. L.Y. acknowledges the support from the BBSRC David Phillips Research Fellowship. E.L. is supported by an ISF grant to E.H.. We thank Dr. Mark Wells for assistance in peptide design and synthesis, Dr. Grace W. Yu for providing MDM2 and Dr. Daniel P. Teufel for providing Taz2.

Materials and Methods

Protein expression, purification and labelling

Human p53 NTD (residues 1-91), p53 NTD plus CD (residues 1-292) and full-length p53 (residues 1-393) were expressed in *Escherichia coli* and purified as described (46, 47). In p53 NTD, two cysteine residues were introduced at either positions 1 and 91, or positions 10 and 56 or positions 56 and 91. All the mutants of NTD plus CD and

flp53 were based on a stabilized mutant with quadruple mutation (48). Exposed Cys (Cys-182, Cys-275 and Cys-227) and the partly buried one (Cys-124) were mutated to Ala. An additional Cys was then introduced into appropriate exposed positions so that fluorophores could be attached to p53 through Cys residues. The Cys residues were labelled with a FRET donor/acceptor pair, either AF488 and AF647 or AF546 and AF647. The proteins were labelled as described (21). After the reaction being quenched with 1 mM β-mercaptoeth`nol, the labelled protein was separated from the free dyes on a G-25 desalting column. No evidence of multiple labelling of the purified protein was observed in mass spectra. The labelling of full-length p53 with ReAsH was carried out in the presence of DTT as described (43). Excess ReAsH was removed on a G-25 desalting column.

Single-Molecule FRET measurements

Details of single molecule experiments have been described (21). In brief, the FRET pair (AF488/AF647 or AF546/AF647) labelled proteins were excited with either the 488 line (for AF488) or 514 line (for AF546) from an Argon ion laser (Model 35LAP321-230, Melles Griot). Fluorescence from the donor and acceptor was separately detected with two photon-counting modules (SPCM-AQR14, Perkin Elmer). All the single-molecule experiments were carried out at 20 °C in phosphate buffer (pH 7) with 20 mM phosphate plus 150 mM NaCl (both highest grade from Sigma-Aldrich). To prevent the labelled protein sticking to the surface of the cover-glass chamber, we added 1 μM of the unlabelled protein to the solution.

Time-resolved FRET measurements

Time-resolved FRET (TR-FRET) experiments were carried out with a single photon counting setup (LifeSpec-ps, Edingburgh Instruments, Edingburgh, UK) with a LED featuring ~500 ps pulse width at 282 nm. The peptides were measured in phosphate

buffer (20 mM Phosphate plus 100 mM NaCl, pH 7) at 50 μM. Details on data analysis are available in Supporting Information.

References

1. Vogelstein B, Lane D, & Levine AJ (2000) Surfing the p53 network. *Nature* 408:307-310.
2. Hainaut P & Wiman K (2005) *25 Years of p53 Research* (Spriner, New York).
3. Clore GM, *et al.* (1995) Refined solution structure of the oligomerization domain of the tumour suppressor p53. *Nature Struct Biol* 2:321-333.
4. Cho Y, Gorina S, Jeffrey PD, & Pavletich NP (1994) Crystal structure of a p53 tumor suppressor-DNA complex: Understanding tumorigenic mutations. *Science* 265:346-355.
5. Dawson R, *et al.* (2003) The N-terminal domain of p53 is natively unfolded. *J Mol Biol* 332:1131-1141.
6. Müller-Tiemann BF, Halazonetis TD, & Elting JJ (1998) Identification of an additional negative regulatory region for p53 sequence-specific DNA binding. *Proc Natl Acad Sci USA* 95:6079-6084.
7. Joerger AC, Hwee CA, Veprintsev DB, Blair CM, & Fersht AR (2005) Structures of p53 cancer mutants and mechanism of rescue by second-site suppressor mutations. *J Biol Chem* 280:16030-16037.
8. Lee W, *et al.* (1994) Solution structure of the tetrameric minimum transforming domain of p53. *Nature Struct Biol* 1:877-890.
9. Tidow H, *et al.* (2007) Quaternary structures of tumor suppressor p53 and a specific p53-DNA complex. *Proc Natl Acad Sci USA* 104:12324-12329.

10. Wells M, *et al.* (2008) Structure of tumour suppressor p53 and its intrinsically disordered N-terminal transactivation domain. *Proc Natl Acad Sci USA* 105:5762-5767.

11. Okorokov AL, *et al.* (2006) The structure of p53 tumour suppressor protein reveals the basis for its functional plasticity. *EMBO J* 25:5191-5200.

12. Weiss S (2000) Measuring conformational dynamics of biomolecules by single molecule fluorescence spectroscopy. *Nat. Struct. Biol.* 7:724-729.

13. Schuler B & Eaton WA (2008) Protein folding studied by single-molecule FRET. *Curr Opin Struc Biol* 18:16-26.

14. Beechem JM & Haas E (1989) Simultaneous determination of intramolecular distance distributions and conformational dynamics by global analysis of energy transfer measurements. *Biophys. J.* 55:1225-1236.

15. Sherman E & Haran G (2006) Coil-globule transition in the denatured state of a small protein. *Proc Natl Acad Sci USA* 103:11539-11543.

16. Laurence TA, Kong X, Jäger M, & Weiss S (2005) Probing structural heterogeneities and fluctuations of nucleic acids and denatured proteins. *Proc Natl Acad Sci USA* 102:17348-17353.

17. Mukhopadhyay S, Krishnan R, Lemke EA, Lindquist S, & Deniz AA (2007) A natively unfolded yeast prion monomer adopts an ensemble of collapsed and rapidly fluctuating structures. *Proc Natl Acad Sci USA* 104:2649-2654.

18. Merchant KA, Best RB, Louis JM, Gopich IV, & Eaton WA (2007) Characterizing the unfolded states of proteins using single-molecule FRET spectroscopy any molecular simulations. *Proc Natl Acad Sci USA* 104:1528-1533.

19. Deniz AA, *et al.* (2000) Single-molecule protein folding: Diffusion fluorescence resonance energy transfer studies of the denaturation of chymotrypsin inhibitor 2. *Proc Natl Acad Sci USA* 97:5179-5184.

20. Schuler B, Lipman EA, & Eaton WA (2002) Probing the free-energy surface for protein folding with single-molecule fluorescence spectroscopy. *Nature* 419:743-747.

21. Huang F, Sato S, Sharpe TD, Ying LM, & Fersht AR (2007) Distinguishing between cooperative and unimodal downhill protein folding. *Proc Natl Acad Sci USA* 104:123-127.

22. Andrecka J, *et al.* (2008) Single-molecule tracking of mRNA exiting from RNA polymerase II. *Proc Natl Acad Sci USA* 105:135-140.

23. Henzler-Wildman KA, *et al.* (2007) Intrinsic motions along an enzymatic reaction trajectory. *Nature* 450:838-844.

24. Sharma S, *et al.* (2008) Monitoring Protein Conformation along the Pathway of Chaperonin-Assisted Folding. *Cell* 133:142-153.

25. Diez M, *et al.* (2004) Proton-powered subunit rotation in single membrane-bound F 0F1-ATP synthase. *Nature Struct Mol Biol* 11:135-141.

26. Mori T, Vale RD, & Tomishige M (2007) How kinesin waits between steps. *Nature* 450:750-754.

27. Majumdar DS, *et al.* (2007) Single-molecule FRET reveals sugar-induced conformational dynamics in LacY. *Proc Natl Acad Sci USA* 104:12640-12645.

28. Kapanidis AN, *et al.* (2004) Fluorescence-aided molecule sorting: Analysis of structure and interactions by alternating-laser excitation of single molecules. *Proc Natl Acad Sci USA* 101:8936-8941.

29. Haas E (2005) The study of protein folding and dynamics by determination of intramolecular distance distributions and their fluctuations using ensemble and single-molecule FRET measurements. *ChemPhysChem* 6:858-870.

30. Joerger AC, Allen MD, & Fersht AR (2004) Crystal structure of a superstable mutant of human p53 core domain: Insights into the mechanism of rescuing oncogenic mutations. *J Biol Chem* 279:1291-1296.

31. Huang F, Settanni G, & Fersht AR (2008) Fluorescence resonance energy transfer analysis of the folding pathway of Engrailed Homeodomain. *Protein Eng Des Sel* 21:131-146.

32. Haran G, Haas E, Szpikowska BK, & Mas MT (1992) Domain Motions in Phosphoglycerate Kinase - Determination of Interdomain Distance Distributions by Site-Specific Labeling and Time-Resolved Fluorescence Energy-Transfer. *Proc Natl Acad Sci USA* 89:11764-11768.

33. Kussie PH, *et al.* (1996) Structure of the MDM2 oncoprotein bound to the p53 tumor suppressor transactivation domain. *Science* 274:948-953.

34. Best RB, *et al.* (2007) Effect of flexibility and cis residues in single-molecule FRET studies of polyproline. *Proc Natl Acad Sci USA* 104:18964-18969.

35. Doose S, Neuweiler H, Barsch H, & Sauer M (2007) Probing polyproline structure and dynamics by photoinduced electron transfer provides evidence for deviations from a regular polyproline type II helix. *Proc Natl Acad Sci USA* 104:17400-17405.

36. Huang F & Nau WM (2003) A conformational flexibility scale for amino acids in peptides. *Angew. Chem. Int. Ed.* 42:2269-2272.

37. Zagrovic B, *et al.* (2005) Unusual compactness of a polyproline type II structure. *Proc Natl Acad Sci USA* 102:11698-11703.

38. Möglich A, Joder K, & Kiefhaber T (2006) End-to-end distance distributions and intrachain diffusion constants in unfolded polypeptide chains indicate intramolecular hydrogen bond formation. *Proc Natl Acad Sci USA* 103:12394-12399.

39. Haas E, Katchalski-Katzir E, & Steinberg IZ (1978) Brownian motion of the ends of oligopeptide chains in solution as estimated by energy transfer between the chain ends. *Biopolymers* 17:11-31.

40. Navon A, Ittah V, Landsman P, Scheraga HA, & Haas E (2001) Distributions of intramolecular distances in the reduced and denatured states of bovine pancreatic ribonuclease A. Folding initiation structures in the C-terminal portions of the reduced protein. *Biochemistry* 40:105-118.

41. Huang F, Hudgins RR, & Nau WM (2004) Primary and secondary structure dependence of peptide flexibility assessed by fluorescence-based measurement of end-to-end collision rates. *J Am Chem Soc* 126:16665-16675.

42. Sakamoto H, Lewis MS, Kodama H, Appella E, & Sakaguchi K (1994) Specific sequences from the carboxyl terminus of human p53 gene product form anti-parallel tetramers in solution. *Proc Natl Acad Sci USA* 91:8974-8978.

43. Adams SR, *et al.* (2002) New biarsenical ligands and tetracysteine motifs for protein labeling in vitro and in vivo: Synthesis and biological applications. *J Am Chem Soc* 124:6063-6076.

44. Hillger F, *et al.* (2008) Probing protein-chaperone interactions with single-molecule fluorescence spectroscopy. *Angew. Chem. Int. Ed.* 47:6184-6188.

45. Rajagopalan S, Andreeva A, Teufel DP, Freund SM, & Fersht AR (2009) Interaction between the Transactivation Domain of p53 and PC4 Exemplifies

Acidic Activation Domains as Single-stranded DNA Mimics. *J Biol Chem* 284:21728-21737.

46. Veprintsev DB, *et al.* (2006) Core domain interactions in full-length p53 in solution. *Proc Natl Acad Sci USA* 103:2115-2119.

47. Yu GW, *et al.* (2006) The central region of HDM2 provides a second binding site for p53. *Proc Natl Acad Sci USA* 103:1227-1232.

48. Nikolova PV, Henckel J, Lane DP, & Fersht AR (1998) Semirational design of active tumor suppressor p53 DNA binding domain with enhanced stability. *Proc Natl Acad Sci USA* 95:14675-14680.

Figure legends

Figure 1. Single-molecule FRET histogram for isolated N-terminal domain (p53NTD) with dyes labelled at various positions as shown in each panel. In the left panels, AF488/AF647 FRET pair was used; in the right panels, AF546/AF647 FRET pair was used. Data were acquired at 20 °C in phosphate buffer (pH 7) with 20 mM phosphate plus 150 mM NaCl.

Figure 2. Distance distribution for synthetic peptides derived from NTD of p53. The distributions were obtained by fitting the time-resolved fluorescence of the donor in the presence of FRET with assumption of single skewed Gaussian distribution. Data were acquired at 20 °C in phosphate buffer (pH 7) with 20 mM phosphate plus 150 mM NaCl.

Figure 3. Single-molecule FRET histogram for the N-terminal domain plus DNA binding core domain (p53NCD). In the top panels, AF488/AF647 FRET pair was used; in bottom panels, AF546/AF647 FRET pair was used. Data were acquired at 20 °C in phosphate buffer (pH 7) with 20 mM phosphate plus 150 mM NaCl.

Figure 4. Single-molecule FRET histogram for full-length p53 (flp53). In the top panels, AF488/AF647 FRET pair was used; in bottom panels, AF546/AF647 FRET pair was used. Data were acquired at 20 °C in phosphate buffer (pH 7) with 20 mM phosphate plus 150 mM NaCl.

Figure 5. Schematic SAXS model of flp53 (9), where the DNA binding core domains (CD) are in green or cyan, the tetramerization domain (TetD) in red, linkers in gray, N-terminal domain (NTD) in salmon and C-terminus in yellow. The red arrows indicate possible interactions between the NTD and CD in the p53 tetramer.

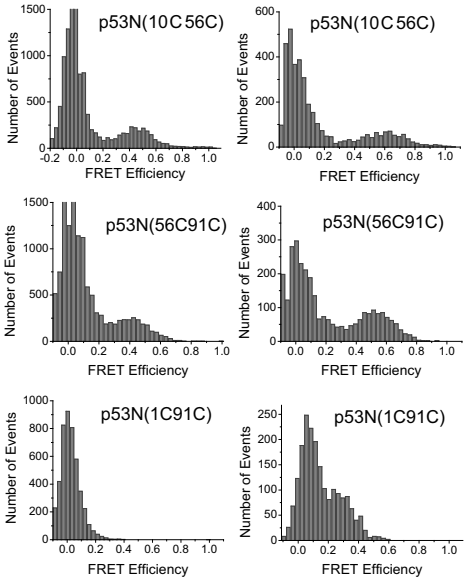
p53N(10C 56C)
Number of Events
FRET Efficiency
p53N(10C 56C)
Number of Events
FRET Efficiency
p53N(56C91C)
Number of Events
FRET Efficiency
p53N(56C91C)
Number of Events
FRET Efficiency
p53N(1C91C)
Number of Events
FRET Efficiency
p53N(1C91C)
Number of Events
FRET Efficiency

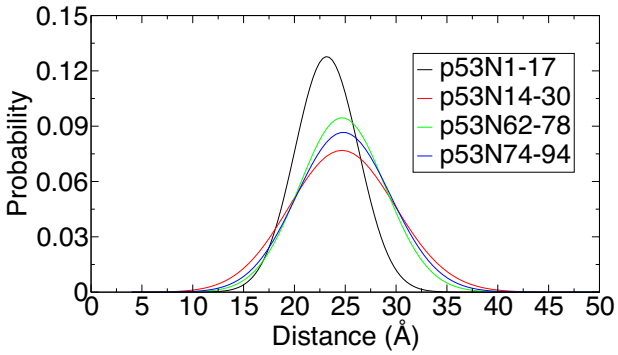
0.15
0.12
0.09
0.06
0.03
0
Probability
0
5
10
15
20
25
30
35
40
45
50
Distance (Å)
p53N1-17
p53N14-30
p53N62-78
p53N74-94

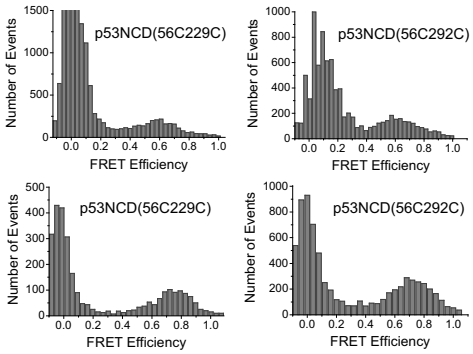
p53NCD(56C229C)
Number of Events
FRET Efficiency
p53NCD(56C292C)
Number of Events
FRET Efficiency
p53NCD(56C229C)
Number of Events
FRET Efficiency
p53NCD(56C292C)
Number of Events
FRET Efficiency

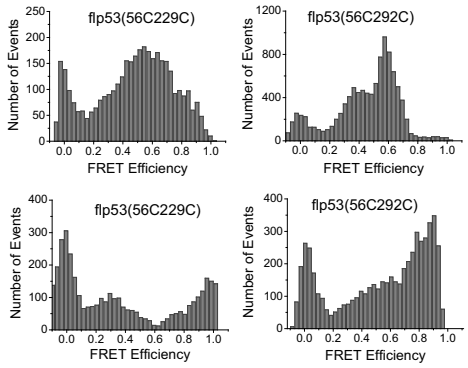
flp53(56C229C)
Number of Events
FRET Efficiency
flp53(56C292C)
Number of Events
FRET Efficiency
flp53(56C229C)
Number of Events
FRET Efficiency
flp53(56C292C)
Number of Events
FRET Efficiency

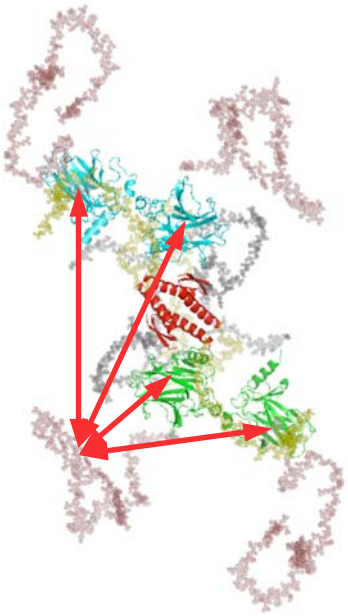

Table 1. Apparent average distances obtained from SM-FRET measurements.*

	p53N(10C56C)	p53N(56C91C)	p53N(1C91C)	p53NCD(56C229C)	p53NCD(56292C)
E_{488647}	0.45	0.40	NA	0.63	0.60
E_{546647}	0.61	0.53	0.25	0.77	0.70
R_{488647} (Å)	54	56	NA	48	49
R_{546647} (Å)	58	62	76	52	55

* $E_{488\text{-}647}$, $E_{546\text{-}647}$, $R_{488\text{-}647}$ and $R_{547\text{-}647}$ are the FRET efficiency and corresponding distance obtained with AF488 and AF546 as donor, respectively. The error in distance is estimated to be 10%, which is the upper limit of the error after considering all the errors in the calculation of Förster distance, the peak position of the histogram and the γ value.

Tabel 2. Parameters of the distance distribution, diffusion coefficient and χ^2 obtained from the fit of TR-FRET data.

	p53N1-17*	p53N14-30	p53N62-78	p53N74-92
Mean (Å)	$22.3^{+0.3}_{-0.5}$	$22.3^{+0.0}_{-0.8}$	$23.2^{+0.3}_{-0.4}$	$23.0^{+0.3}_{-0.5}$
Standard Deviation (Å)	$3.2^{+0.8}_{-1.4}$	$5.4^{+0.4}_{-0.0}$	$4.4^{+0.2}_{-1.4}$	$4.8^{+0.3}_{-1.1}$
Diffusion Coefficient (Å^2/ns)	$0.0^{+0.1}_{-0.0}$	$0.0^{+0.2}_{-0.0}$	$0.4^{+0.0}_{-0.3}$	$0.6^{+0.0}_{-0.4}$
χ^2	1.24	1.28	1.48	1.24

*The error on the parameters is defined by the projection of the region in parameter space where $\chi^2 < 1.05\times \chi^2_{min}$

Multiple conformations of full-length p53 detected with single-molecule fluorescence resonance energy transfer

Supporting Information

Control experiments

Extensive control experiments, including protein and DNA binding, fluorescence correlation spectroscopy and time-resolved fluorescence anisotropy, were carried out to test for possible structural and functional effects of the mutations and labelling modifications that might have influenced the conclusions derived from the FRET experiments.

Functionality and structure of labelled protein

To look for any influence of the dye labels on the properties of p53, we checked whether the binding affinities of the labelled NTD with Mdm2 and Taz2 proteins were appreciably affected. AF488/AF647 doubly labelled p53N10C56C had dissociation constants of 200 nM and 25 nM with Mdm2 and Taz2, respectively, which were very similar to those for unlabelled p53 NTD peptides (160 nM and 27 nM with Mdm2 and Taz2, respectively) (1). The dissociation constant of the AF488 labelled protein with consensus response element DNA (5' AF647-TGAGGAACATGTCCCAACATGTTGAGCTC 3') was 60 nM for flp5356C229C, which was similar to that for wild-type p53 with the same DNA (2). The control experiments suggest that the dyes had little effect on the protein functionality and structure.

Fluorescence correlation spectroscopy (FCS)

To exclude the possibility that the multiple peaks in the SM-FRET efficiency histogram were due to aggregation of proteins, we measured the diffusion time of the

p53 mutants with fluorescence correlation spectroscopy (FCS). The experiments were carried out with a confocal fluorescence microscope similar to that used for the single-molecule FRET experiments under the same conditions but with 10 nM labelled protein. Typical FCS decay curves are shown in Fig. S2. The diffusion time for different mutants varies between 0.2 ms to 0.6 ms (an acceptable range). No extraordinarily slow diffusing species were observed in all cases, suggesting that there were no aggregates in the samples.

Time-resolved anisotropy experiments

Fluorescence anisotropy decays were recorded using time-correlated single photon counting techniques as described elsewhere (3-6). Excitation of the donor was achieved using a picosecond amplified and frequency doubled diode laser (490nm 100ps pulse width) operating at 5MHz (PicoTA, Picoquant Germany). Excitation of the acceptor at 615nm was undertaken using the pulse-picked output (3.8 MHz sub 1 ps) of an optical parametric oscillator (Coherent Mira OPO USA), synchronously pumped by a 76 MHz mode locked Ti:Sapphire laser (Mira 900F & Verdi V10, Coherent USA). Fluorescence measurements were carried out at ca 2 μM concentrations at room temperature (21-22°C) in 50 μL quartz fluorescence cuvettes (Hellma, Essex, UK). Fluorescence was detected by a microchannel plate photomultiplier (R3809U Hamamatsu, Japan), using a right-angled excitation-detection geometry with the appropriate choice of filters. For donor fluorescence measurements, a 531±11 nm band pass filter (Semrock USA) was employed. Acceptor fluorescence was detected through an OG530 and RG665 long pass filter combination. A quartz Glan Taylor polariser (Karl Lambrecht Corp. USA) was used to produce vertically polarised (0º) excitation pulses. An analysing sheet polariser (CVI-Melles USA) was sequentially altered between 0º (vertical, V) and 90º

(horizontal, H) to obtain the polarised intensity measurements $I_V(t)$ and $I_H(t)$, here t denotes the excitation–detection coincidence time measured by the TCSPC system. The fluorescence intensities $I(t)$ and emission anisotropies $r(t)$ were determined from $I(t) = I_V(t) + 2I_H(t)$ and $r(t) = \left(I_V(t) - I_H(t)\right) \Big/ \left(I_V(t) + 2I_H(t)\right)$, respectively.

Time-resolved fluorescence anisotropy decays were measured for all the mutants by exciting the donor and observing the emission of the donor and the acceptor, or by exciting the acceptor directly and observing the emission of the acceptor. To determine the behaviour of the fluorescence anisotropy of the donor in the absence of FRET, two donor-only labelled p53 mutants were also studied. One mutant was labelled at position 56 and the other labelled at position 229. These mutants have only one exposed cysteine at position 56 or 229, respectively. All the mutants show a bi-exponential anisotropy decay with a very fast component (< 1 ns) and a relatively slow decay (~3 ns to 10 ns) (See Fig. S3). The slow components in the time-resolved anisotropy decay were hard to determine accurately because of the short fluorescence lifetimes (~ 2 ns) and therefore contain relatively large errors. The fast decay component can be attributed to the fast local rotation of the bound fluorophores and the slow decay represents the segmental flexibility or the tumbling of the protein as a whole. The amplitude of the fast components is indicative that both donor and acceptor molecules are free to undergo significant internal orientational relaxation and that it is reasonable to assume the κ^2 to be 2/3 in the calculation of Förster distance (7, 8). This also indicates that the multiple peaks in the single molecule FRET efficiency histogram do not arise from restricted fluorophores, as reported in previous work for a different system (9). It is also notable that the fluorescence anisotropy for all the mutants has decayed to zero within ~ 25 ns, which further supports the absence of aggregates in the sample.

Time-resolved FRET data analysis

The time-resolved FRET data were fitted to Equation 1 numerically:

$$\frac{\partial}{\partial t}g_{\mathrm{N}}^{*}(r,t)=-\frac{1}{\tau_0}\left(1+\left(\frac{R_0}{r}\right)^6\right)g_{\mathrm{N}}^{*}(r,t)+D\frac{1}{r^2}\frac{\partial}{\partial r}r^2\frac{\partial}{\partial r}g_{\mathrm{N}}^{*}(r,t)+D\frac{1}{r^2}\frac{\partial}{\partial r}\left(r^2 g_{\mathrm{N}}^{*}(r,t)\frac{\partial}{\partial r}\beta U(r)\right) \quad (1)$$

where D is the mutual intramolecular end-to-end diffusion constant, the sum of the diffusion coefficients of the two ends. β^{-1} is the product of the Boltzman constant and temperature ($\beta = 1/k_{\mathrm{B}}T$), and $U(r)$ is the potential energy of the chain possessing an end-to-end distance r. If the ground-state equilibrium radial distribution function $g_{\mathrm{N}}(r)$ is known, the potential energy can be obtained according to Equation 2, assuming no perturbation of the distribution function upon excitation of the donor (8, 10).

$$\beta U(r)=-\ln g_{\mathrm{N}}(r) \quad (2)$$

Equation 1 can be used to calculate the survival probability density of an excited state at distance r subject to the boundary conditions:

$$\frac{\partial}{\partial r}g_N^{*}(r,t)+g_N^{*}(r,t)\frac{\partial}{\partial r}\beta U(r)\Big|_{r=r_{\min}}=0 \quad (3a)$$

$$\frac{\partial}{\partial r}g_N^{*}(r,t)+g_N^{*}(r,t)\frac{\partial}{\partial r}\beta U(r)\Big|_{r=r_{\max}}=0 \quad (3b)$$

In the present work TR-FRET data were fitted assuming a normally distributed $g_{\mathrm{N}}(r)$**:**

$$g_{\mathrm{N}}(r)=\frac{1}{\sigma\sqrt{2\pi}}\exp\left(-\frac{(r-r_0)^2}{2\sigma^2}\right) \quad (4)$$

Thus, the free parameters of the fit are r_0, σ and D. For each trial set of parameters, the differential Eq. 1 was solved numerically, using the boundary conditions Eq.3.

The Gaussian chain model (or random coil model) has also been used for comparison. In that case the radial distribution function is:

$$g_N(r) = \left(\frac{3}{2\pi\sigma^2}\right)^{3/2} \exp\left(-\frac{3(r)^2}{2\sigma^2}\right) \quad (5)$$

The theoretical fluorescence decay was convoluted with the experimental instrument response function and compared with experimental data. The least squares fit was accomplished by minimizing the mean squared deviation (χ^2) between time-resolved FRET data and the theoretical model using the Levenberg-Marquardt algorithm. The error on the parameters was assigned using the projections of the region of parameter space where $\chi^2 < 1.05 \times \chi^2_{min}$. The latter was sampled using a Monte-Carlo procedure in the parameter space with χ^2 as energy function, and temperature and step size allowing a 30% acceptance ratio.

Calculation of Förster critical distance

The Förster critical distance, R_0, was calculated for each FRET pair with equation 6

$$R_0 = 0.211\left[\kappa^2 n^{-4} Q_D J\right]^{1/6} \quad (6)$$

where κ^2 is the dipole orientation factor and assumed to be 2/3; n is the refractive index of the solution measured experimentally; Q_D is the fluorescence quantum yield of the donor and obtained from the donor-labeled protein, with reported fluorescence quantum yield from Invitrogen for corresponding free dye as reference; J is the overlap of the emission spectrum of the protein-labelled donor and the absorption spectrum of the protein-labelled acceptor. Dyes labelled on p53NCD(56C91C) and flp53(56C229C) were used to calculate the Förster critical distances. Owing to very similar fluorescence quantum yields and spectra obtained for dyes labelled on these two protein constructs, the same R_0 values within error were obtained. The Förster distance for Nal/EDANS was calculated with fluorophores labelled in the p53N1-17 peptide and assumed to be the same for the other two peptides with the same pair. The

Förster distance for EDANS/Dabcyl was based on the fluorophores labelled in the p53N14-30 peptide.

Data analysis for SM-FRET experiments

FRET efficiencies (E) of each burst were calculated according to $E = (n_A)/(n_A + \gamma n_D)$, where n_A, and n_D are the background corrected photon counts from the acceptor and donor, respectively, and γ is the constant to correct the difference in fluorescence quantum yield of the donor and acceptor and the detection efficiency of the detectors for the donor and acceptor. For the used FRET pairs and the current setup, $\gamma \approx 1$. To calculate the γ value, the fluorescence quantum yield of the labelled dyes were measured and the relative detection efficiency of the donor and acceptor channels was determined by comparing the FRET efficiency of DNA sample labelled with the same donor/acceptor pair with 100% labelling efficiency obtained from the confocal setup and from a calibrated fluorometer. The peak position of the histogram with single peak was determined by fitting the histogram with a double Gaussian distribution ($y = A_1 \exp\left(-\frac{(x-x_1)^2}{2\sigma_1^2}\right) + A_2 \exp\left(-\frac{(x-x_2)^2}{2\sigma_2^2}\right) + C$), for the Zero peak and the real FRET peak.

Distance calculation for steady-state FRET experiments

The FRET in AF488/ReAsH system was determined by steady-state fluorescence intensity, i.e., $E = (I_D - I_{DA})/I_D$, where E, I_D and I_{DA} are the FRET efficiency, fluorescence intensity of AF488 in the absence and presence of ReAsH, respectively. The distance between dyes (r) was then calculated with $r = (1/E - 1)^{1/6} R_0$.

Peptide synthesis

Peptides p53N1-17 (residues 1-17 : (Asp-EDANS)-MEEPQSDPSVEPPLSQE-(Nal-Ala)), p53N14-30 (residues 14-30: (Asp-EDANS)-LSQETFSDLWKLLPENN-

(Dabcyl-Lys)), p53N62-78 (residues 62-78: (Asp-EDANS)-EAPRMPEAAPPVAPAPA-(Nal-Ala)) and p53N74-92 (residues 74-92: Asp-EDANS)-APAPAAPTPAAPAPAPS-(Nal-Ala)-P)) were synthesized on a Pioneer peptide synthesizer (Applied Biosystems) using standard Fmoc chemistry. Naphthylalanine, EDANS and Dabsyl were incorporated into the peptides during solid phase peptide synthesis using Fmoc-1-Nal-OH, Fmoc-Asp(EDANS)-OH and Fmoc-Lys(Dabsyl)-OH (all from Bachem, UK), respectively. All other amino acids were purchased from NOVAbiochem. The peptides were purified on a Waters HPLC using a reverse-phase C8 semipreparative column (Vydac) as described.(11) All the peptides were lyophilized and had a purity of > 95%.

Protein-protein and protein-DNA binding

To measure the binding constant of NTD of p53 with MDM2 and Taz2, we added MDM2 or Taz2 to 10 nM AF488-labelled NTD. The fluorescence anisotropy was plotted versus titrant concentration, and fitted to a 1:1 binding model (1). The determination of p53-DNA binding constants were carried out as described for double-stranded DNA labelled with AF488 (2).

Circular dichroism measurements

Circular dichroism spectra of the peptides were acquired in phosphate buffer (20 mM Phosphate plus 100 mM NaCl, pH 7) at concentration ranging from 20 to 40 μM on a J-815 CD Spectrometer (JASCO, Tokyo, Japan). The CD spectra were shown in Fig. S4.

References:

1. Teufel, D. P., Freund, S. M., Bycroft, M. & Fersht, A. R. (2007) Four domains of p300 each bind tightly to a sequence spanning both transactivation subdomains of p53. *Proc Natl Acad Sci USA* **104,** 7009-7014.

2. Weinberg, R. L., Veprintsev, D. B. & Fersht, A. R. (2004) Cooperative binding of tetrameric p53 to DNA. *J Mol Biol* **341,** 1145-1159.

3. Bain, A. J., Chandna, P., Butcher, G. & Bryant, J. (2000) Picosecond polarized fluorescence studies of anisotropic fluid media. II. Experimental studies of molecular order and motion in jet aligned rhodamine 6G and resorufin solutions. *J Chem Phys* **112,** 10435-10449.

4. Marsh, R. J., Armoogum, D. A. & Bain, A. J. (2002) Stimulated emission depletion of two-photon excited states. *Chem Phys Lett* **366,** 398-405.

5. White, S. S., Li, H., Marsh, R. J., Piper, J. D., Leonczek, N. D., Nicolaou, N., Bain, A. J., Ying, L. & Klenerman, D. (2006) Characterization of a single molecule DNA switch in free solution. *J Am Chem Soc* **128,** 11423-32.

6. Chadborn, N., Bryant, J., Bain, A. J. & O'Shea, P. (1999) Ligand-dependent conformational equilibria of serum albumin revealed by tryptophan fluorescence quenching. *Biophys J* **76,** 2198-207.

7. Wu, P. & Brand, L. (1992) Orientation factor in steady-state and time-resolved resonance energy transfer measurements. *Biochemistry* **31,** 7939-7947.

8. Haas, E., Katchalski-Katzir, E. & Steinberg, I. Z. (1978) Effect of the orientation of donor and acceptor on the probability of energy transfer involving electronic transitions of mixed polarization. *Biochemistry* **17,** 5064-5070.

9. Hillger, F., Hänni, D., Nettels, D., Geister, S., Grandin, M., Textor, M. & Schuler, B. (2008) Probing protein-chaperone interactions with single-molecule fluorescence spectroscopy. *Angew. Chem. Int. Ed.* **47,** 6184-6188.

10. Szabo, A., Schulten, K. & Schulten, Z. (1980) First Passage Time Approach to Diffusion Controlled Reactions. *J. Chem. Phys.* **72,** 4350-4357.

11. Friedler, A., Hansson, L. O., Veprintsev, D. B., Freund, S. M. V., Rippin, T. M., Nikolova, P. V., Proctor, M. R., Rüdiger, S. & Fersht, A. R. (2002) A peptide that binds and stabilizes p53 core domain: Chaperone strategy for rescue of oncogenic mutants. *Proc Natl Acad Sci USA* **99,** 937-942.

Figure S1. Time-resolved fluorescence spectrum. Shown are the time-resolved fluorescence (black), the instrument response function (green), deconvoluted fit (red) and the fitting residual (bottom, black).

Figure S2. Typical FCS curves. Shown are the FCS curves for (a) p53N56C91C, (b) p53NCD56C229C, (c) flp5356C229C and (d) flp5356C292C, which were fitted by assuming there is a single diffusion component and a fast photophysicsisics process. The experiments confirmed the absence of aggregates.

Figure S3. Typical time-resolved fluorescence anisotropy decay curves. (a) flp5356C labelled with AF546 at position 56; (b) flp53229C labelled with AF488 at position 229; (c) the donor signal for flp5356C292C labelled with both AF546 and AF647; (d) the acceptor signal in the presence of FRET for flp5356C292C labelled with both AF546 and AF647; (e) the donor signal for flp5356C229C labelled with both AF488 and AF647; (f) the acceptor signal in the presence of FRET for flp5356C229C labelled with both AF488 and AF647. The faster relaxation decay is an indication of no restricted fluorophore motions and absence of aggregates.

Figure S4. Circular dichroism spectra for peptides derived from the NTD of p53.

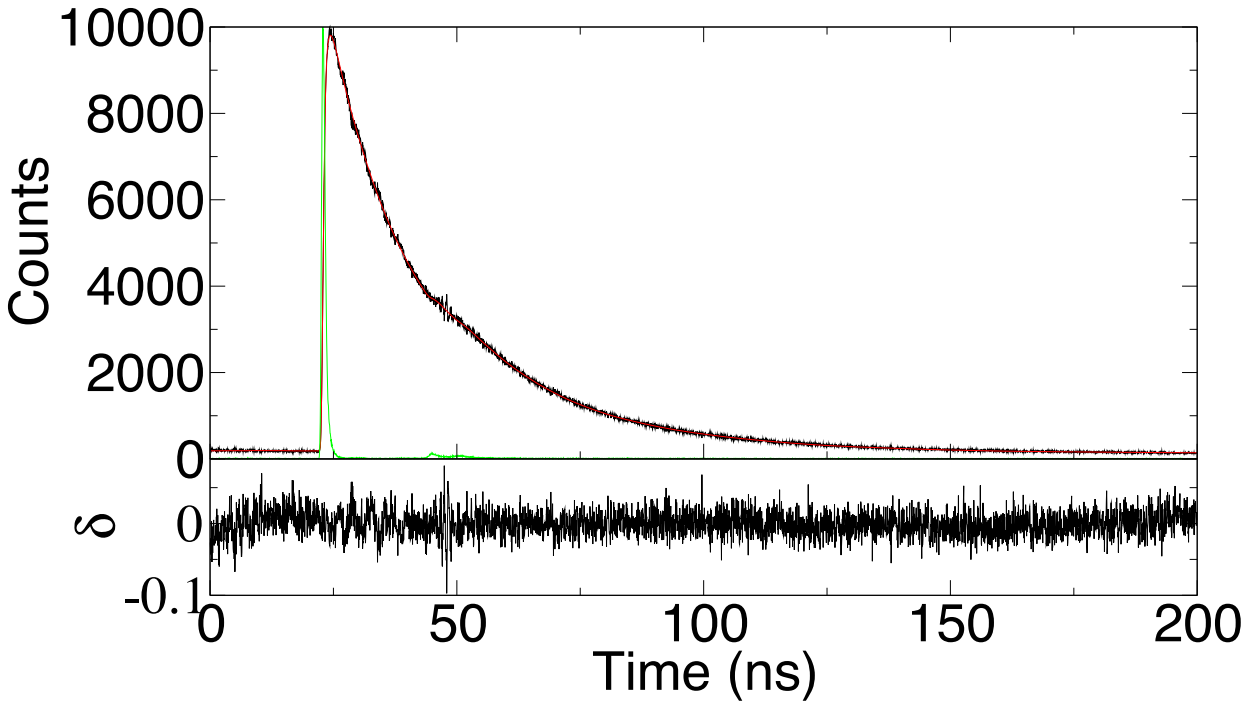
10000
8000
6000
4000
2000
0
Counts
0
δ
-0.1
0
50
100
150
200
Time (ns)

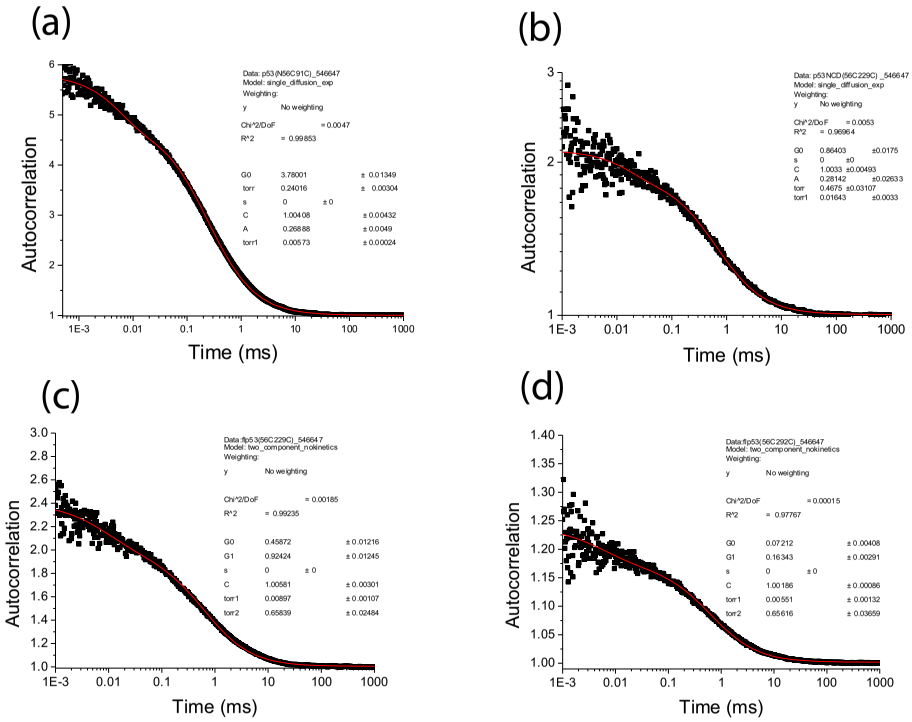
(a)
Data: p53 (N56C91C)_546647
Model: single_diffusion_exp
Weighting:
y No weighting
Chi^2/DoF = 0.0047
R^2 = 0.99853
G0 3.78001 ± 0.01349
torr 0.24016 ± 0.00304
s 0 ± 0
C 1.00408 ± 0.00432
A 0.26888 ± 0.0049
torr1 0.00573 ± 0.00024
Autocorrelation
Time (ms)
(b)
Data: p53 NCD (56C229C) _546647
Model: single_diffusion_exp
Weighting:
y No weighting
Chi^2/DoF = 0.0053
R^2 = 0.96964
G0 0.86403 ±0.0175
s 0 ±0
C 1.0033 ±0.00493
A 0.28142 ±0.02633
torr 0.4675 ±0.03107
torr1 0.01643 ±0.0033
Autocorrelation
Time (ms)
(c)
Data: flp53(56C229C)_546647
Model: two_component_nokinetics
Weighting:
y No weighting
Chi^2/DoF = 0.00185
R^2 = 0.99235
G0 0.45872 ± 0.01216
G1 0.92424 ± 0.01245
s 0 ± 0
C 1.00581 ± 0.00301
torr1 0.00897 ± 0.00107
torr2 0.65839 ± 0.02484
Autocorrelation
Time (ms)
(d)
Data:flp53(56C292C)_546647
Model: two_component_nokinetics
Weighting:
y No weighting
Chi^2/DoF = 0.00015
R^2 = 0.97767
G0 0.07212 ± 0.00408
G1 0.16343 ± 0.00291
s 0 ± 0
C 1.00186 ± 0.00086
torr1 0.00551 ± 0.00132
torr2 0.65616 ± 0.03659
Autocorrelation
Time (ms)

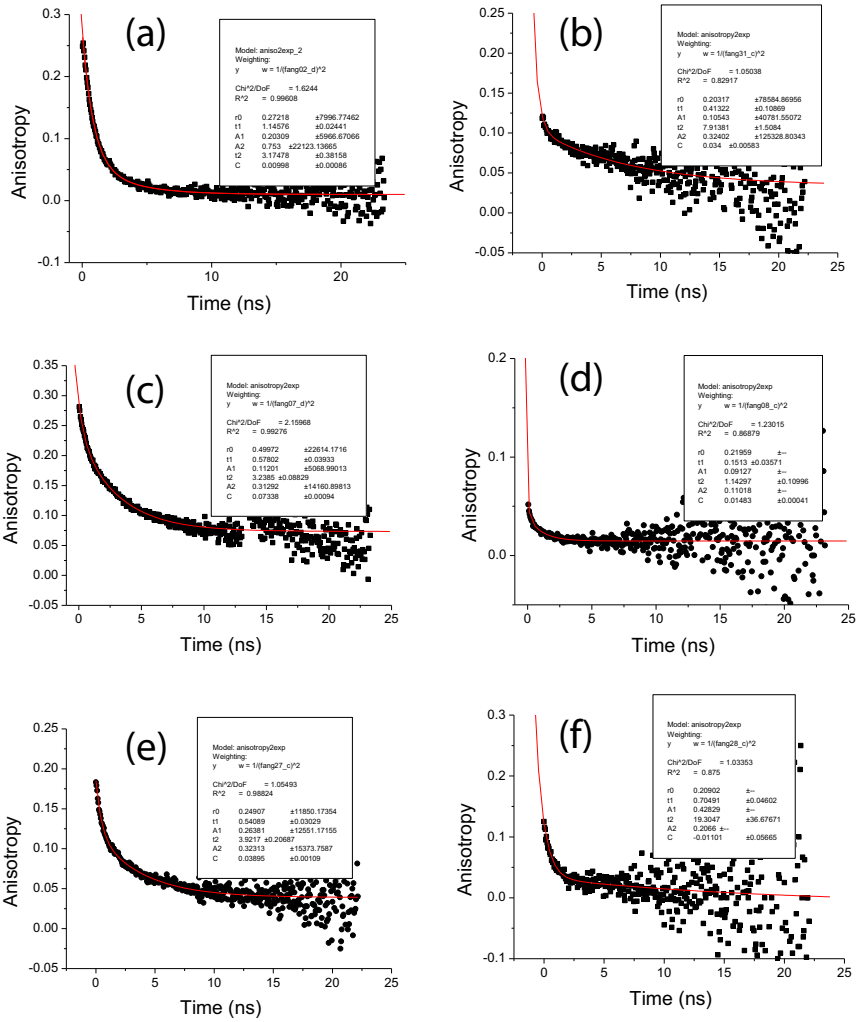
(a)
Model: aniso2exp_2
Weighting:
y w = 1/(fang02_d)^2
Chi^2/DoF = 1.6244
R^2 = 0.99608
r0 0.27218 ±7996.77462
t1 1.14576 ±0.02441
A1 0.20309 ±5966.67066
A2 0.753 ±22123.13665
t2 3.17478 ±0.38158
C 0.00998 ±0.00086
(b)
Model: anisotropy2exp
Weighting:
y w = 1/(fang31_c)^2
Chi^2/DoF = 1.05038
R^2 = 0.82917
r0 0.20317 ±78584.86956
t1 0.41322 ±0.10869
A1 0.10543 ±40781.55072
t2 7.91381 ±1.5084
A2 0.32402 ±125328.80343
C 0.034 ±0.00583
(c)
Model: anisotropy2exp
Weighting:
y w = 1/(fang07_d)^2
Chi^2/DoF = 2.15968
R^2 = 0.99276
r0 0.49972 ±22614.1716
t1 0.57802 ±0.03933
A1 0.11201 ±5068.99013
t2 3.2385 ±0.08829
A2 0.31292 ±14160.89813
C 0.07338 ±0.00094
(d)
Model: anisotropy2exp
Weighting:
y w = 1/(fang08_c)^2
Chi^2/DoF = 1.23015
R^2 = 0.86879
r0 0.21959 ±--
t1 0.1513 ±0.03571
A1 0.09127 ±--
t2 1.14297 ±0.10996
A2 0.11018 ±--
C 0.01483 ±0.00041
(e)
Model: anisotropy2exp
Weighting:
y w = 1/(fang27_c)^2
Chi^2/DoF = 1.05493
R^2 = 0.98824
r0 0.24907 ±11850.17354
t1 0.54089 ±0.03029
A1 0.26381 ±12551.17155
t2 3.9217 ±0.20687
A2 0.32313 ±15373.7587
C 0.03895 ±0.00109
(f)
Model: anisotropy2exp
Weighting:
y w = 1/(fang28_c)^2
Chi^2/DoF = 1.03353
R^2 = 0.875
r0 0.20902 ±--
t1 0.70491 ±0.04602
A1 0.42829 ±--
t2 19.3047 ±36.67671
A2 0.2066 ±--
C -0.01101 ±0.05665
Anisotropy
Time (ns)

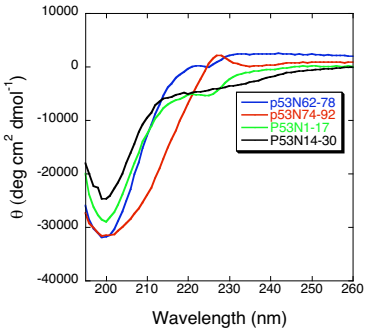
10000
0
-10000
-20000
-30000
-40000
θ (deg cm^2 dmol^{-1})
200
210
220
230
240
250
260
Wavelength (nm)
p53N62-78
p53N74-92
P53N1-17
P53N14-30

Tabel S1. Parameters of the distance distribution, diffusion coefficient and χ^2 obtained from the fit of TR-FRET data with the program developed by Haas and colleagues (Haran, G., Haas, E., Szpikowska, B. K., and Mas, M. T. *Proc Natl Acad Sci USA* **89,** 11764-11768 (1992)).

	p53N1-17*	p53N14-30	p53N62-78	p53N74-92
Mean (Å)	$22.3^{+3.8}_{-0.3}$	$26.5^{+1.9}_{-0.0}$	$25.5^{+0.8}_{-1.1}$	$24.4^{+0.4}_{-0.5}$
Standard Deviation (Å)	$5.4^{+10.8}_{-0.0}$	$11.1^{+2.1}_{-0.6}$	$10.9^{+0.5}_{-1.7}$	$7.2^{+0.0}_{-1.1}$
Diffusion Coefficient (Å^2/ns)	0.3-1	0-2.9	0-0.3	0-0.1
χ^2	1.423	1.148	1.271	1.297